Structure and Dynamics of 9(10H)-Acridone and Its Hydrated Clusters. III. Microscopic Solvation Effects on Nonradiative Dynamics

Masaaki Mitsui,† Yasuhiro Ohshima,* and Okitsugu Kajimoto‡

Department of Chemistry, Graduate School of Science, Kyoto University, Kitashirakawa-Oiwakecho, Sakyo-ku, Kyoto 606-8502, Japan

Received: March 20, 2000; In Final Form: July 5, 2000

As the final part of the series, nonradiative dynamics and energy-level structure of relevant electronic excited states in 9(10H)-acridone (AD) and its hydrated clusters have been studied by various spectroscopic methods. Time-resolved fluorescence measurements on their $^1(\pi,\pi^*)$ origin excitation have revealed that the fluorescence decay is very fast (≈10 ps) for bare AD but drastically lengthened (> ns) in AD−$(H_2O)_n$ ($n = 1-6$ and higher). Bare AD has been observed clearly by mass-selective delayed ionization and sensitized-phosphorescence detection, which indicates the efficient formation of molecules in triplet manifold after the $^1(\pi,\pi^*)$ excitation. Several weak peaks have been identified around each $^1(\pi,\pi^*)$ vibronic band of bare AD, and they are attributed to $^3(n,\pi^*)$ transitions which borrow intensity from the nearby $^1(\pi,\pi^*)$ bands through the direct spin−orbit coupling. Such satellite bands completely disappear in the fluorescent cluster spectra with $n \geq 1$. All of the experimental observations indicate that the dominant nonradiative pathway in bare AD is the $S_1(\pi,\pi^*) \rightarrow T_2(n,\pi^*)$ intersystem crossing (ISC) followed by the $T_2(n,\pi^*) \rightarrow T_1(\pi,\pi^*)$ internal conversion. This direct ISC process becomes prohibited by the energy-level inversion between the S_1 and T_2 states induced by the H bonding to the C═O site. Thus the relaxation pathway is "switched" to the second-order ISC [$S_1(\pi,\pi^*) \rightarrow T_1(\pi,\pi^*)$] in the fluorescent hydrated clusters, where the carbonyl site is involved in H-bonding networks. Owing to the increasing S_1-T_2 separation, the fluorescence quantum yield becomes larger for the higher clusters, which is approaching to the bulk solution value, i.e., $\Phi_f \approx 1$. The (π,π^*) and (n,π^*) shifts at each cluster geometry have been calculated as (N)HOMO−LUMO gaps in DFT orbital energies to support the picture on the energy-level structure. Most importantly, a small falloff in the fluorescence decay constants from $n = 2$ to 3 has been definitely correlated to the crossover in H-bonding topologies (the C═O bonded → the bridged form), which has already been established in papers I and II. The delayed ionization has identified new spectral features that are completely absent in the fluorescence excitation spectrum. They are assigned to the N−H bonded isomer(s) with $n \leq 3$, which is at least as stable as the C═O bonded conformer(s) with the same size. The ISC in the hydrate(s) should be as fast as in bare AD, because of the lack of the S_1-T_2 level inversion. These experimental findings demonstrate the site-specific solvation effects on the electronic energy-level structure and the resultant nonradiative dynamics in the hydrated clusters of a bifunctional molecule.

1. Introduction

Nonradiative photophysical processes of 9(10H)-acridone (AD) are strongly affected by solvation. There have been a number of studies on the electronic relaxation processes of AD in condensed phase,[1−5] and it has been established that its nonradiative decay is governed by intersystem crossing (ISC) and the decay rate is sensitive especially to the H-bonding ability of solvent molecules. Consequently, the fluorescence lifetime of AD is extremely short in aprotic solvents at room temperature (e.g., ≤ 300 ps in cyclohexane),[1] while it becomes substantially longer in protic solvents (e.g., ≈12 ns in ethanol).[1,5] The pronounced solvation effects on the ISC rate in AD have been explained in terms of relative energy ordering of two excited states, i.e., $S_1(\pi,\pi^*)$ and $T_2(n,\pi^*)$, as shown in Figure 1. In

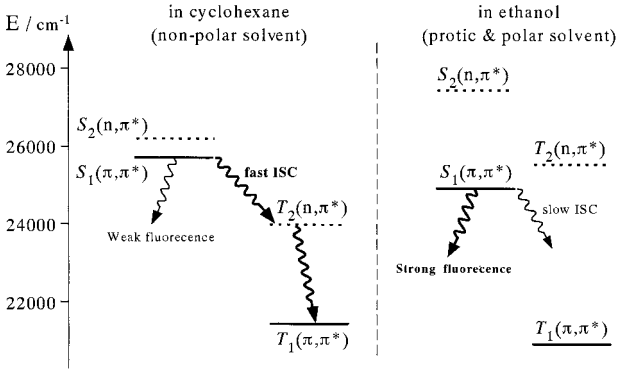

Figure 1. Energy level diagram explaining solvation effects on the fluorescence property of acridone in nonpolar solvents (left) and polar solvents (right).

cyclohexane (as a nonpolar solvent), the strongly allowed transition to the $^1(\pi,\pi^*)$ state has been identified at ≈25900 cm^{-1}, whereas the $T_2(n,\pi^*)$ state has been predicted to be located around 2000 cm^{-1} below $S_1(\pi,\pi^*)$. Therefore, the rapid

* Corresponding author. Fax: +81-75-753-3974. E-mail: ohshima@kuchem.kyoto-u.ac.jp.

† Research Fellow of the Japan Society for the Promotion of Science for Young Scientists, 1997−1999.

‡ Also Core Research for Evolutional Science and Technology (CREST), Japan Science and Technology Corporation (JST).

10.1021/jp001049u CCC: $19.00
Published on Web 08/31/2000

$S_1(\pi,\pi^*) \rightarrow T_2(n,\pi^*)$ ISC process, in accord with El-Sayed's rule,[6−8] i.e., *direct* ISC, takes place in nonpolar solvents and, as a result, the fluorescence quantum yield of AD is extremely small (e.g., 0.015 in cyclohexane).[1] On the other hand, in ethanol (as a protic and polar solvent), the $S_1(\pi,\pi^*)$ state is shifted to lower energy whereas the $T_2(n,\pi^*)$ state is largely destabilized through the H-bonding effects, resulting in the energy ordering reversal for the $S_1(\pi,\pi^*)$ and $T_2(n,\pi^*)$ states. This level inversion makes the $S_1 \rightarrow T_2$ direct ISC channel prohibited and strong fluorescence is observed in this class of solvent: the fluorescence quantum yield of AD in ethanol is 0.97.[1] These arguments clearly indicate that the modification of electronic-energy structure by microscopic H-bonding is of crucial importance to solvation effects upon nonradiative dynamics in AD.

In the first two papers of this series, we have elucidated the water solvation structures in the hydrated AD clusters, and we are now ready to discuss how and why the local H bonding affects the ISC process which is operative in AD. In this final paper in the series, we present the nonradiative dynamics of bare AD and these hydrated clusters explored by several spectroscopic methods. Picosecond time-resolved measurements have shown pronounced increase in fluorescence lifetime by microscopic solvation, which resembles the liquid-phase behavior of AD. Delayed ionizaion[9−12] and sensitized-phosphorescence excitation (SPE),[13] established as sensitive techniques for detecting triplet molecules, have been applied in order to figure out the energy ordering for the participating electronic states. These methods have confirmed the predominance of ISC in relaxation pathways and also revealed a spectroscopic evidence for direct S−T coupling in AD under isolated conditions. Based upon the results thus obtained and those presented in the preceding papers (I and II), molecular-level interpretation for solvation effects on nonradiative dynamics of AD will be addressed.

2. Experimental Section

2.1. Fluorescence-Based Laser Spectroscopy. The apparatus and procedures for fluorescence-excitation (FE) and UV−UV hole-burning (HB) measurements have already been described in paper I. Picosecond time-resolved fluorescence spectroscopy has been performed by employing the time-correlated single photon counting (TC-SPC) method. Details of the TC-SPC setup have been presented elsewhere.[14] The experiment was performed with a mode-locked Ti:saphire laser (Spectra Physics, Tsunami 3950; 82 MHz repetition rate, 1.4 ps fwhm) pumped by a cw Ar^+ laser (Spectra Physics, Beamlok 2060, 6 W) for picosecond pulse excitation. Wavelength of the laser output was measured within ±0.1 nm accuracy by a wavemeter (Advantest, TQ8325). The repetition rate of the laser was reduced to 10−20 MHz by using an electrooptical modulator (ConOptics, #350−160) and was focused onto a $LiIO_3$ crystal to generate the second harmonic. The resultant UV light was crossed with a supersonic expansion at a position 15−20 mm downstream from a heated pulsed nozzle, which was operated at 30−50 Hz with ≈2 ms gas-pulse duration. Fluorescence from samples in the jet was collected by a pair of lenses onto a multichannel plate photomultiplier tube (MCP-PMT; Hamamatsu, C2773). A sharp-cut filter (Schott, GG375, GG385, and so on) was placed in front of the MCP-PMT to block the scattered light of the excitation pulse. The output of the MCP-PMT was preamplified, pulse-shaped by a constant fraction discriminator (CFD; Tennelec, TC454), and finally fed into a picosecond time analyzer (PTA; EG&G, #9308) as a start pulse. To reduce the background noise, the CFD was gated so as to synchronize the most cooled part of the gas pulse with ≈1 ms duration. The residual fundamental of the laser light was detected by a fast photodiode, whose output was also processed by the CFD and used as a stop pulse for the PTA. Temporal response of the detection system was monitored as the UV light scattered by a thin wire, which was flipped into the laser-jet interaction region before and after the fluorescence measurements. The obtained response function, whose fwhm was typically 40 ps, was used for the analysis of fluorescence time profiles. Observed fluorescence decay curves were fitted by the nonlinear least-squares method with a monoexponential function convoluted with the response function.

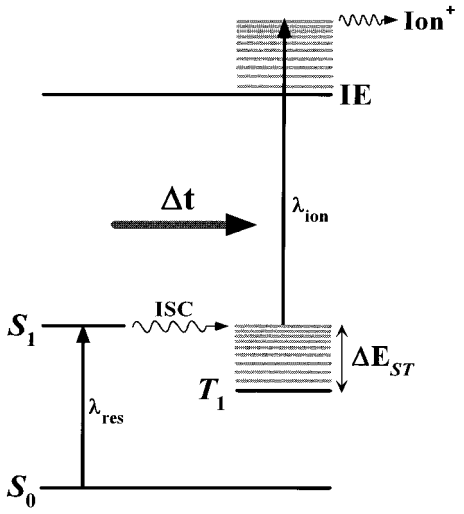

Figure 2. Schematic energy level diagram for delayed ionization.

2.2. Delayed Ionization Mass Spectrometry. In the present study, two-color resonance-enhanced two-photon ionization (2C-R2PI) mediated through triplet manifold, often called "delayed ionization",[9−12] has been performed for bare AD and its hydrated clusters under supersonic expansion conditions. The delayed ionization is a sensitive technique to detect nonfluorescent molecules which have efficient ISC processes, and its utility has been shown for several molecular systems.[9−12] The experimental setup for the delayed ionization experiment presented here is almost the same as that of the 2C-R2PI experiment described in paper I, and thus only important points are mentioned here. Until now, most of the delayed ionization experiments have been carried out by utilizing the combination of a frequency-tunable dye laser for resonance pulse (λ_{res}) and an ArF excimer laser at 193 nm for ionization pulse (λ_{ion}). In the present work, two independent frequency-tunable dye lasers were used as resonance and ionization sources. This flexible irradiation setup enabled us to measure photoionization yield curves via triplet manifold. A schematic energy diagram for delayed ionization spectrometry is shown in Figure 2. The interval between the two laser pulses (Δt) was controlled by a digital delay/pulse generator (SRS, DG535). In measurements of excitation spectra, the λ_{ion} was delayed by typically 100 ns ($= \Delta t$) with respect to λ_{res} and fixed at frequency high enough to proceed ionization. In time profile measurements, both the λ_{ion} and λ_{res} were fixed, and Δt was scanned.

2.3. Sensitized Phosphorescence Excitation Spectroscopy. A detection system for sensitized phosphorescence excitation (SPE) spectroscopy[13] was newly constructed and attached to the setup for fluorescence-based laser spectroscopy.[15] In our apparatus, a copper plate with an area of ≈25 cm^2 was placed 60 mm downstream from the nozzle at an angle of 45° against the jet stream. The plate was kept cooled at liquid-nitrogen

TABLE 1: Solvation Shifts, Fluorescence Lifetimes, and Fluorescence Quantum Yields for Acridone and Its Hydrated Clusters

species	solvation shift[a]/cm^{-1}	τ_f/ns	Φ_f [b]
A (bare AD)	0	0.01	4.0×10^{-4}
B ($n = 1$)	−472	2.3	0.08
C ($n = 2$)	−740	10.9	0.40
D ($n = 3$)	−1364	7.7	0.28
E ($n = 4$)	−1589	15.0	0.55
F ($n = 5$)	−1649	19.2	0.71
H ($n = 6$)	−1851	23.0	0.85
N ($n \geq 7$)	−2155	24.0	0.88

[a] Relative to the origin band of bare AD at 27265 cm^{-1}. [b] Obtained as τ_f/τ_r^{vac}, where τ_r^{vac} is estimated as described in the text and assumed to be constant for all the species.

temperature. In this experiment, biacetyl (BA) was employed as phosphor because of the relatively small phosphorescence quantum yield of AD. Vapor of BA was introduced as 10 Hz gas pulses from another pulsed valve, which was located near the cold plate surface. Sensitized phosphorescence emission from the phosphor surface was focused onto a photomultiplier tube (PMT; Hamamatsu, R585) through a set of quartz lenses. Appropriate color filters (Schott, GG395 and GG435) were placed in front of the PMT to block the strong scattered light of the UV laser. The output from the PMT was preamplified and fed into a gated photon counter (SRS, SR400). The output of the photon counter was digitized by a 13-bit A/D converter and stored in a personal computer. The background noise was discriminated to be less than 10 counts/s. In the measurement of SPE spectra, the time gate with ≈100 μs duration was fixed ≈20 μs after the laser pulse. Other experimental details were the same for the FE measurements described in paper I.

3. Results

3.1. Fluorescence Lifetimes of AD and Its Hydrated Clusters. Fluorescence decays were measured for the $^1(\pi,\pi^*)$ origins of AD−$(H_2O)_n$, i.e., species A−F ($n = 0-5$), H ($n = 6$), and N ($n \geq 7$). All of the observed decay profiles were fitted well to a single-exponential function by nonlinear-least squares regressions ($\chi^2 < 1.2$). The fluorescence lifetimes thus obtained are listed in Table 1 and are also plotted against the solvation shifts of the clusters in Figure 3. For bare AD (species A), the lifetime is extremely short (≈10 ps), so that its time profile is almost instrumentally limited. We have checked that the signal is not due to the scattered light: photon counts became negligibly small if the excitation wavelength was slightly (≈0.5 nm) off from the resonance. The lifetime shows 200-fold increase from bare AD to the $n = 1$ cluster (species B), and is further lengthened by a factor of 5 by addition of another water (species C). It is interesting that the value becomes slightly smaller for $n = 3$ (species D), and again gradually increases for the larger clusters. For $n = 6$ (species H) or larger, the lifetime seems to be converging at ca. 25 ns. It has been reported that the pure radiative lifetime of AD is 13.4 ns in ethanol.[16] The radiative lifetime in a vacuum, τ_r^{vac}, is related to the value in solution, τ_r^{sol}, as $\tau_r^{vac} = n^2\tau_r^{sol}$, where n is the refractive index of solution.[17,18] Thus τ_r^{vac} of AD is estimated to be 27.2 ns by adopting the τ_r^{sol} and the refractive index (1.367)[16] for ethanol solution. Fluorescence quantum yields (Φ_f) for each cluster are evaluated from the observed lifetimes and the estimated τ_r^{vac}, as listed in Table 1. It is apparent that Φ_f is negligibly small for bare AD but becomes substantially larger, which is approaching to unity as increasing degrees of hydration.

3.2. Spectroscopy of Bare AD. As has been mentioned in paper I, we have not been able to detect ions of bare AD by 2C-R2PI when we excited the molecules into the region just above the vertical ionization energy of AD (7.69 eV).[19] This must be due to the extremely fast decay after excitation into its $^1(\pi,\pi^*)$ origin just mentioned in section 3.1. If the relaxation process in isolated AD molecules proceeds via ISC, as has been claimed in solution,[1−5] 2C-R2PI manifested through triplet manifold should be applicable for detecting bare AD. Thus, we scanned the ionization laser (λ_{ion}) into a shorter wavelength region (<260 nm), as the excitation laser (λ_{res}) was fixed to the $^1(\pi,\pi^*)$ origin band. The photoionization yield curve thus obtained is indicated in Figure 4a. As has been shown, ions in the AD^+ mass channel appeared at ≈259 nm and gradually increased as the λ_{ion} became shorter. The total ion signal showed no appreciable change for delay times ranging between 1 ns−1 μs. This observation confirms that the ionization of bare AD is proceeded via triplet manifold, since the lifetime of the initially

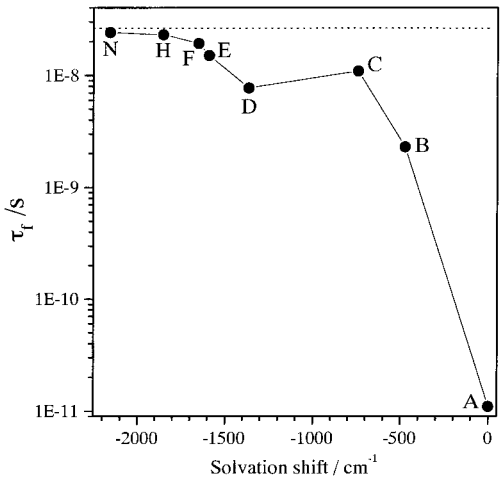

Figure 3. Fluorescence decay constants for the observed AD−$(H_2O)_n$ clusters (species A−F, H, and N) against their spectral shifts relative to the monomer electronic origin. Species A−F are bare AD, the C=O bonded $n = 1$ and 2, and the bridged $n = 3-5$, respectively. H is an $n = 6$ cluster probably with a cyclic water bridge (see Figure 7 of paper II), and N for $n \geq 7$.

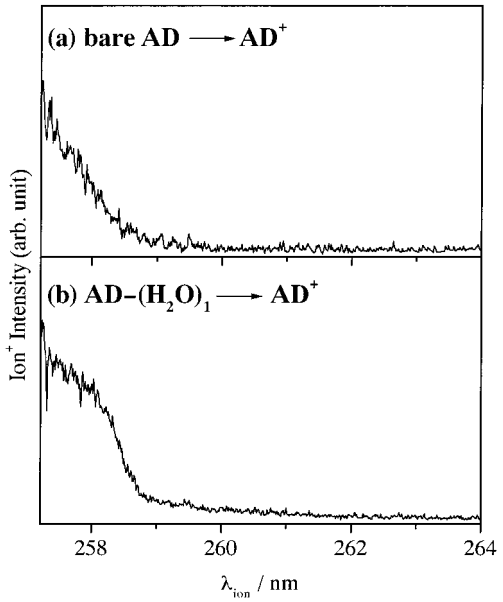

Figure 4. Photoionization yield curves via triplet manifold for: (a) bare AD and (b) AD−$(H_2O)_1$ of the C=O bonded form, plotted against the ionization wavelength. The excitation laser was set at resonance with the $^1(\pi,\pi^*)$ origin bands. The time delay between λ_{res} and λ_{ion} was set to 100 ns for both measurements.

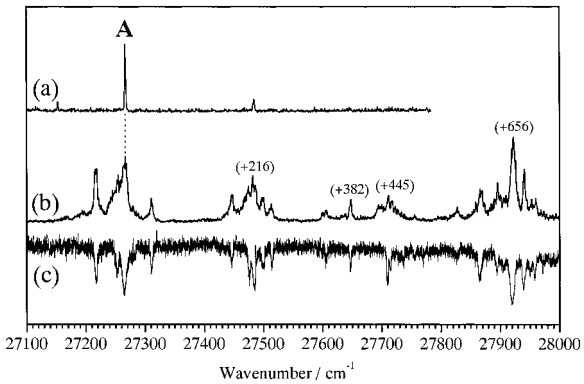

Figure 5. Excitation spectra of bare AD obtained by (a) fluorescence excitation, (b) delayed ionization monitoring at the mass-channel of 195 amu (i.e., AD^+ mass), and (c) hole-burning by probing the depletion in the origin-band fluorescence. Spectra b and c have been recorded with strong excitation or burn laser pulses, and thus suffer from saturation effects. Note that a weak peak at 27160 cm^{-1} appearing in spectrum a is a vibronic band of species B [$AD-(H_2O)_1$].

excited singlet state is extremely short (≈10 ps) as mentioned above. Thus the lifetime of the triplet state AD monomer should be longer than 1 μs. For further longer delay times (>1 μs), the ion signal decreased probably due to the escape of the AD molecules from the detection region. It is noted that the decay corresponding to the singlet-state lifetime of AD is too fast to be observed with the present experimental setup employing ns lasers.

The excitation spectrum of bare AD was also measured by the delayed ionization for comparison with that taken by the FE measurement. In the FE spectrum, only two weak bands are observed for bare AD as shown in Figure 5a. The stronger band at 27265 cm^{-1} is assigned to the electronic origin of the $^1(\pi,\pi^*)$ transition and the weaker one at 27481 cm^{-1} as the lowest totally symmetric mode (+216 cm^{-1} relative to the origin). When the laser power of λ_{res} was kept as low as possible to avoid saturation effects, the spectrum obtained by the delayed ionization was almost the same as the FE spectrum, several vibronic bands were also observed in a higher frequency region (>500 cm^{-1} above the origin). This implies that the nonradiative decay becomes even faster as the molecule gains more vibrational excitation in the $^1(\pi,\pi^*)$ state. By employing the λ_{res} with stronger power, the excitation spectrum shows significantly different features as indicated in Figure 5b. This spectrum was recorded by monitoring the AD^+ mass channel with the λ_{ion} fixed at 255 nm and delayed by 100 ns with respect to the λ_{res}. A number of peaks are observed in vicinity of the vibronic bands which have already been located in the FE and low-power R2PI spectra. We further performed the UV−UV HB measurement to identify these satellite peaks. Figure 5c shows the HB spectrum obtained by setting the probe laser pulse on resonance to the bare AD origin band and scanning the intense burn laser pulse. As clearly seen, the HB and delayed-ionization spectra are essentially the same, indicating that all the peaks in the spectra are due to a single species, i.e., the AD monomer. As a further confirmation, we carried out the SPE measurement on bare AD, and also obtained a spectrum (not shown) essentially identical to the spectra shown in Figures 5b and 5c. Relative intensities of the observed bands in the spectra are much distorted by the saturation effects, and the satellite bands should be much weaker than the main vibronic bands. Failure to observe by the FE measurement sets the intensities of the satellites well below 1/100 of the origin band. These satellite bands should originate from some interstate coupling between other nearby electronic state(s) and are discussed more

TABLE 2: $S_1(\pi,\pi^*)$ State Vibrational Levels and Assignments for Acridone

$\Delta\nu^a/cm^{-1}$	assignment	$\Delta\nu^a/cm^{-1}$	assignment
−49	satellite	382	a_1
−12	satellite	445	a_1
0	origin	561	?
45	satellite	602	216+382
180	satellite	629	satellite
208	satellite	656	a_1
216	a_1	674	a_1
233	satellite	687	satellite
247	satellite	693	satellite

[a] Relative to the origin band at 27265 cm^{-1}.

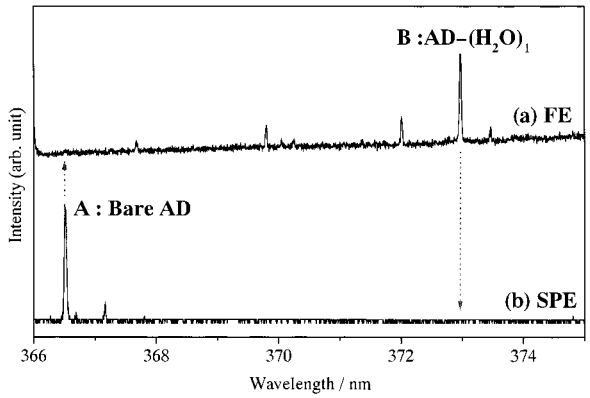

Figure 6. Excitation spectra simultaneously recorded by (a) fluorescence and (b) sensitized phosphorescence detection. The origin bands for bare AD (band A) and $AD-(H_2O)_1$ (band B) are indicated.

detail in section 4.2. Transition frequencies and assignments of prominent bands shown in Figures 5b and 5c are summarized in Table 2. The vibronic assignments in the $^1(\pi,\pi^*)$ state are carried out by consulting the DFT normal-mode analysis for the S_0 state. It was found that only totally symmetric (a_1) modes had appreciable intensity in the $^1(\pi,\pi^*)$ transition system.

We also carried out a search for other vibronic features in bare AD over 2000 cm^{-1} to the red of the $^1(\pi,\pi^*)$ origin by both the hole-burning and delayed ionization methods with strong burn or resonance laser pulse (up to several mJ/pulse), which completely saturated the $^1(\pi,\pi^*)$ transitions. However, we did not find any signal in the region thus examined.

3.3. Spectroscopy of Hydrated AD Clusters. Figure 6 shows FE and SPE spectra simultaneously recorded with a moisturized gas sample for the $^1(\pi,\pi^*)$ origin region of bare AD and $AD-(H_2O)_1$ (species B). In the FE spectrum, the origin band of bare AD was observed extremely weak but that of $AD-(H_2O)_1$ was strong, whereas in the SPE spectrum the bare AD band was strong and the $AD-(H_2O)_1$ band was not observed at all. This exactly opposite behavior clearly demonstrates that the remarkable increase in fluorescence quantum yields of the AD chromophore is interpreted in terms of the microscopic solvation effect on the ISC process.

As has been mentioned in paper I, the hydrated clusters of AD with $n = 1-6$ (species B−F and H) have been detected by 2C-R2PI via singlet manifold. Though the ISC rates are not so fast as in bare AD, species B and C ($n = 1$ and 2, respectively) have been able to be ionized also via triplet manifold: by using λ_{ion} short enough, ions from these clusters were observed even with a longer delay time (up to ≈1 μs). In this case, signals were detected only in fragment channels with one water loss, i.e., AD^+ for species B and $AD^+-(H_2O)_1$ for species C. Photoionization yield curves for both the species show an onset at ≈259 nm as bare AD. The curve for species B is shown in

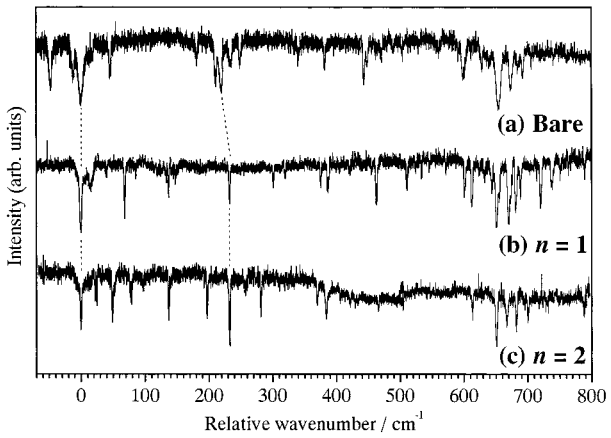

Figure 7. Hole burning spectra of (a) bare AD (species A), (b) AD−$(H_2O)_1$ (species B), and (c) AD−$(H_2O)_2$ (species C) plotted in relative shifts from their origin bands (27265, 26793, and 26525 cm^{-1}, respectively).

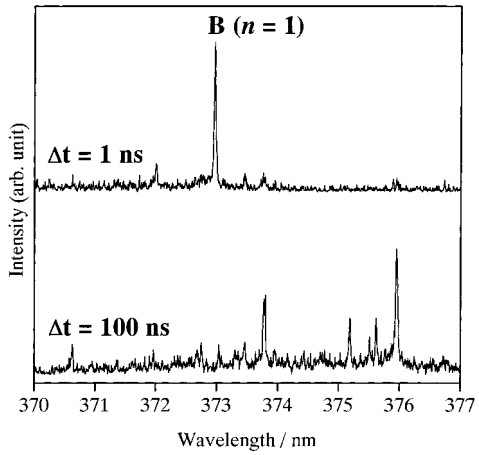

Figure 8. Excitation traces recorded by monitoring the AD−$(H_2O)_1^+$ mass channel with $\lambda_{ion} = 270$ nm and the delay times between λ_{res} and λ_{ion} set to (a) 1 ns and (b) 100 ns. In trace (b), several new bands due to hydrated AD cluster(s) with $n \geq 1$ are apparent. It is noted that they have never been observed in the FE spectrum.

Figure 4b; it arises more steeply at the onset than that for bare AD. The signal for species C was too weak for detailed comparison. The fragmentation observed after the delayed ionization should take place in the neutral state, since the clusters after the ISC are vibrationally hot and predissociation may occur in the triplet manifold.[12] This is in contrast to the fragmentation of species C after ionization via singlet manifold, which proceeds in the ionic state as discussed in paper I. The steeper rise for species B is probably because the triplet AD molecules formed by the predissociation of the $n = 1$ cluster lose a certain vibrational energy so as to be relatively "cooler" than those generated after photoexcitation of bare AD followed by the fast ISC.

UV−UV HB measurements have been performed to figure out whether the hydrated clusters also exhibit satellite peaks in their $^1(\pi,\pi^*)$ transition as bare AD. Figure 7a−c shows the close-up of HB traces near the origin region for bare AD, $n = 1$ (species B), and $n = 2$ (species C), respectively. A number of low-frequency vdW modes are observed in the spectra for the hydrated clusters, but there are no features which can be assigned to satellite bands originating from the interstate coupling as in bare AD. A broad and weak band (fwhm ≈10 cm^{-1}) was observed at only 15 cm^{-1} above the origin in the HB spectrum of $n = 1$, but it should not be a satellite for the following reason. The FE measurement on the 1:1 hydrate of a substituted AD molecule, i.e., *N*-methyl-acridone, has identified a weak band +18 cm^{-1} above its $^1(\pi,\pi^*)$ origin.[20] The cluster geometry has been confirmed as a C═O bonded type,[20] which is similar to AD−$(H_2O)_1$ **I** (species B), thus the observed low-frequency bands are ascribed to vdW modes with the same character. We note that satellite peaks are not observed in the HB spectra of the other higher hydrates (species D−N), either.

3.4. Detection of Nonfluorescent Hydrated AD Clusters. The delayed ionization has revealed the existence of new hydrated AD cluster(s), which cannot be detected by the fluorescence-based or singlet-manifold ionization method, as briefly mentioned in papers I and II. Figure 8 shows two excitation spectra in the 370−377 nm region recorded by monitoring the AD−$(H_2O)_1^+$ mass channel with fixing $\lambda_{ion} =$ 270 nm. Only the delay times (Δt) between λ_{res} and λ_{ion} were set to much different conditions: $\Delta t \approx 1$ ns for the upper spectrum, whereas $\Delta t \approx 100$ ns for the lower spectrum. Completely different excitation spectra were obtained under such two conditions. In the upper spectrum, all resonances are due to the $^1(\pi,\pi^*) \leftarrow S_0$ transition of the AD−$(H_2O)_1$ cluster (species B) as with Figure 2b in paper I. Ions detected in the parent AD−$(H_2O)_1^+$ channel are produced after ionization via the $^1(\pi,\pi^*)$ manifold, as the signals disappeared for $\Delta t > 20$ ns. On the other hand, several new bands which have never been observed in the FE spectrum appear in the lower spectrum. These bands can be observed for delay times up to ≈ 1 μs, confirming that the carrier(s) of the new bands should be ionized via triplet manifold. These observations indicate that (almost) nonfluorescent hydrated AD cluster(s) ($n \geq 1$) are also formed with substantial abundance in the supersonic expansion. As bare AD, they proceed fast ISC into the triplet manifold after photoexcitaion into the $^1(\pi,\pi^*)$ state. At the present stage, definitive mass assignments cannot be achieved because ionization via triplet manifold inevitably accompanies fragmentation as mentioned in section 3.3.

4. Analysis and Discussion

4.1. Energetics of Electronic Excited States in Bare AD. *Singlet Electronic Manifold.* The present study has established that the $^1(\pi,\pi^*)$ transition of AD is located at 27 265 cm^{-1} under isolated conditions. The corresponding absorption in nonpolar solvents, e.g., cyclohexane[1] and benzene,[3] has been identified at around 26 000 cm^{-1}. The red shift in the $^1(\pi,\pi^*)$ transition induced by nonpolar solvents is ca. 1300 cm^{-1}, which is in the same order as other aromatic molecules, e.g., anthracence and its derivatives.[17] In liquid solutions, the lowest singlet excited state (S_1) of AD has been assigned to the $A_1(\pi,\pi^*)$ state irrespective of solvent property.[1−5] The $S_2(n,\pi^*)$ state is predicted to be located 1000−2000 cm^{-1} higher in energy than $S_1(\pi,\pi^*)$ in nonpolar solvents.[1−5] Considering the $^1(\pi,\pi^*)$ blue shift of ≈1300 cm^{-1} from in-solution to isolated conditions, the energy ordering between the two states [$^1(\pi,\pi^*)$ and $^1(n,\pi^*)$] might be reversed in an isolated AD molecule. The $^1(n,\pi^*)$ transition is symmetry forbidden ($A_2 \leftarrow A_1$) for planar C_{2v} structure, but vibronic bands with A_2 or B_2 vibrational symmetry gain finite oscillator strength via vibronic coupling with the nearby $^1A_1(\pi,\pi^*)$ state or another much intense $^1B_1(\pi,\pi^*)$ state located at ≈250 nm,[21] respectively. In the case of other aromatic carbonyls including xanthone (also with C_{2v} symmetry), where $^1(n,\pi^*)$ is known to be well below $^1(\pi,\pi^*)$ from solution studies, the $^1(n,\pi^*)$ transition has been clearly observed also under isolated conditions by phosphorescence excitation,[22−24] SPE,[13,25,26] or delayed-ionization[10] measurements. On the contrary, as

mentioned in section 3.2, no vibronic feature has been observed in the region down to 2000 cm^{-1} below the $^1(\pi,\pi^*)$ origin for bare AD. Since detection sensitivity of the present experiments should be at least comparable to the previous studies, it is highly improbable that the $^1(n,\pi^*)$ origin is located below that of $^1(\pi,\pi^*)$. Another possible assignment for the $^1(n,\pi^*)$ state would be the satellite peaks around the $^1(\pi,\pi^*)$ vibronic bands in its origin region, but this seems to be unlikely for the following reasons. First, the number of satellite peaks is too large and the spacing is so irregular as vibronic bands in the $^1(n,\pi^*)$ origin region. Even when the molecule is distorted into a nonplanar form in (n,π^*), density of states near the origin cannot be so high as the observed satellites. Second, if the $^1(\pi,\pi^*)$ and $^1(n,\pi^*)$ states were quite close each other, vibronic coupling between them should be so extensive that the coupled $^1(n,\pi^*)$ bands would gain substantial intensities. Such strongly interacting bands have been often observed in aromatic molecules with closely located $^1(n,\pi^*)$ and $^1(\pi,\pi^*)$ states.[10,27−30] However, the observed satellites are much weaker than 1% of the $^1(\pi,\pi^*)$ bands in the present case. These arguments suggest that the satellites arise from interstate coupling with a state other than the $^1(n,\pi^*)$ state, and further discussion will be presented in section 4.2. We can also rule out that the $^1(n,\pi^*)$ state may contribute appreciably to the nonradiative dynamics in the $^1(\pi,\pi^*)$ origin region.

Triplet-Electronic Manifold. In the delayed ionization experiment, the λ_{ion} must be set at a shorter wavelength so as to ionize molecules in vibrationally excited states of the triplet manifold populated through ISC.[9] The energy required for the ionization of triplet molecules [E(total)] is approximately equal to the ionization energy (IE) plus the singlet−triplet energy separation (ΔE_{ST}), i.e., $E(\text{total}) = \text{IE} + \Delta E_{ST}$, as schematically shown in Figure 2. The singlet-state lifetime of bare AD was too short to determine its IE by employing 2C-R2PI via singlet manifold. Fortunately, the HeI photoelectron study by Ishijima et al.[19] has settled the vertical ionization energy of AD to be ≈62000 cm^{-1}. Therefore, we can estimate ΔE_{ST} of bare AD by adopting E(total) determined from the photoionization threshold of the triplet AD molecules. As the ionization yield curve measured with the $^1(\pi,\pi^*)$ origin excitation ($\nu_{res} = 27265$ cm^{-1}) represents an onset at ≈259 nm as shown in Figure 4a, E(total) is ≈65800 cm^{-1}. Hence, ΔE_{ST} of bare AD was roughly estimated to be ca. 3800 cm^{-1}, which locates the lowest excited triplet state (T_1) of bare AD at ≈23400 cm^{-1}. Owing to the uncertainty in the IE and the wide Franck−Condon envelop due to the high energy content of the T_1 manifold after the ISC process, the error in the estimated ΔE_{ST} will amount to a several hundred cm^{-1}. In liquid phase, the energy separation between $S_1(\pi,\pi^*)$ and $T_1(\pi,\pi^*)$ has been reported to be ≈3300 cm^{-1}, irrespective of the solvent nature.[5] This value agrees reasonably well with the estimated ΔE_{ST} of AD under isolated conditions, judging from the relatively large uncertainties. The S−T energy separation with the same electronic configuration is basically affected little when isolated or in solution, thus we conclude that T_1 of bare AD is also the (π,π^*) state. It is noted that the $S(\pi,\pi^*)-T(\pi,\pi^*)$ separation of AD (≈3800 cm^{-1}) is much smaller than that of other aromatics such as anthracene (>10 000 cm^{-1}).[8] The smaller value for AD can be explained by the nature of its lowest (π,π^*) configuration. The (π,π^*) excitation is of intramolecular charge-transfer type, and thus considerable local charge migrates from the N−H to C═O group (see Figure 9 in paper I).[21] Such a large change in electronic distribution results in a small electron-exchange integral between the π and π^* orbitals.

The extremely rapid ISC in the $S_1(\pi,\pi^*)$ state of bare AD strongly suggests that the $^3(n,\pi^*)$ state is located between the $S_1(\pi,\pi^*)$ and $T_1(\pi,\pi^*)$ states. This fact is further supported by the observation of satellite peaks, which will be discussed in more detail in section 4.2. At the present stage, the exact location of the $T_2(n,\pi^*)$ state in bare AD has not been clarified. However we can roughly estimate its location by consulting the results on other aromatic carbonyl compounds under jet-cooled conditions,[26] which have shown that the S−T splitting for the (n,π^*) configuration is typically 1000−2000 cm^{-1}. In the case of bare AD, the $^1(n,\pi^*)$ state should lie above the $S_1(\pi,\pi^*)$ state so that the $T_2(n,\pi^*)$ state is expected to be located ≤ 2000 cm^{-1} below the $S_1(\pi,\pi^*)$ origin. Such higher-lying "dark" triplet states (T_n) play an important role in photophysical and photochemical processes of various molecules, and detailed characterization, e.g., exact location, structure, and vibrations, is an interesting subject for further study.

4.2. Interstate Coupling and Nonradiative Dynamics of Bare AD. *Origin of Satellite Bands.* The striking feature observed in the $^1(\pi,\pi^*)$ transition of bare AD is the existence of many satellite peaks around the vibronic bands. The most probable implication is that the $^1(\pi,\pi^*)$ state is coupled with a low-lying (n,π^*) electronic state whose vibronic bands come to appear by borrowing the intensity from the intense $^1(\pi,\pi^*)$ transition. Either singlet or triplet state with the (n,π^*) configuration can be involved in the interstate coupling because of relatively large coupling matrix elements; $^1(\pi,\pi^*)$ and $^1(n,\pi^*)$ can mix with each other through vibronic (pseudo Jahn−Teller) interaction, while $^1(\pi,\pi^*)$ and $^3(n,\pi^*)$ can couple via direct spin−orbit coupling (SOC).[8,31] As the $^1(n,\pi^*)$ state has been located above the $S_1(\pi,\pi^*)$ state in the present case, the only possible origin is the $S_1(\pi,\pi^*)-T_2(n,\pi^*)$ SOC. As is well known theoretically,[31] the z spin sublevel of a $^3A_2(n,\pi^*)$ state in a molecule with C_{2v} symmetry can couple with $^1A_1(\pi,\pi^*)$ states through the one-center SOC (z is parallel to the C═O bond axis), so that the "forbidden" $^3A_2(n,\pi^*) \leftarrow S_0$ transition possesses a finite oscillator strength. The oscillator strength for the triplet transitions (i.e., satellites) becomes appreciably large only for a small energy gap and a large SOC matrix element between the S_1 and T_2 vibronic levels. The latter requires sets of vibrational quantum numbers in the two levels to be similar for a favorable Franck−Condon overlap. Thus the satellites around the $S_1(\pi,\pi^*)$ origin should be T_2 vibronic levels with low vibrational excitation (often denoted as low-v levels). Considering the calculated harmonic frequencies of bare AD in S_0, density of states (DOS) for vibrational fundamentals may be several per 100 cm^{-1} in 1000−2000 cm^{-1} excitation energy, which is of the same order as the number of the satellites around one S_1 vibronic band. As intensity of the satellites is $\leq 10^{-2}$ of the main peak with energy separation of ≤50 cm^{-1}, SOC matrix elements for the satellites are estimated to be ≤1 cm^{-1}. This value is much smaller than the pure electronic SOC matrix element between $^1(\pi,\pi^*)$ and $^3(n,\pi^*)$ in AD, ≈40 cm^{-1}, which is evaluated in accord with Sidman's method by using STO-3G molecular orbitals.[31] When this pure electronic matrix element is adopted, the oscillator strength at the T_2 origin is estimated as $\leq 10^{-3}$ of the S_1 value for $\Delta E(S_1-T_2) \approx$ 1000−2000 cm^{-1}. This exceeds the detection limit of the present HB and delayed ionization methods and rationalizes the unsuccessfulness for observing any vibronic feature below the S_1 origin.

Mechanism of Fast ISC at Electronic Origin. The extremely weak fluorescence after the $^1(\pi,\pi^*)$ excitation of AD under isolated conditions is similar to its fluorescence behavior in nonpolar solvents: the fluorescence quantum yield (Φ_f) of AD

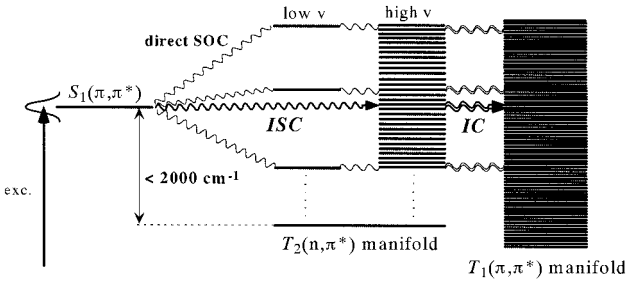

Figure 9. Schematic representation for interstate coupling and nonradiative relaxation processes among the $S_1(\pi,\pi^*)$, $T_2(n,\pi^*)$, and $T_1(\pi,\pi^*)$ states in bare AD. A zeroth order S_1 vibronic level initially prepared by picosecond excitation relaxes into isoenergetic highly excited vibrational levels in the T_2 manifold via the first-order intersystem crossing (ISC), followed by the internal conversion (IC) to the more dense T_1 manifold. The direct S_1-T_2 spin−orbit coupling (SOC) also causes the intensity borrowing for low-v T_2 levels, which appear as satellite peaks around the S_1 vibronic level.

is quite small in nonpolar solvents (e.g., 0.015 in cyclohexane)[1] owing to the rapid ISC from the $^1(\pi,\pi^*)$ state to the $^3(n,\pi^*)$ state. As mentioned in section 3.1, the nonradiative decay rate of the S_1 origin in bare AD is $\approx 10^{11}$ s^{-1}, and this decay is ascribed mostly to the ISC from the initially prepared $S_1(\pi,\pi^*)$ level to the background $T_2(n,\pi^*)$ manifold. In Figure 9 we present the relevant coupling scheme and relaxation pathway of bare AD. The population in the $S_1(\pi,\pi^*)$ origin prepared with picosecond pulse excitation depopulates isoenergetically to the vibronic levels in the $T_2(n,\pi^*)$ manifold via direct ISC, followed by the rapid IC process from the intermediate T_2 manifold to the much more dense T_1 manifold. Though the final product (i.e., bare AD in the T_1 manifold) has indeed been detected by the delayed ionization, no definitive description can be made of the $T_2 \rightarrow T_1$ IC process at this moment. We note that low-v levels in the T_2 manifold that correspond to the satellite peaks do *not* directly contribute to the ISC dynamics explored in the present time-resolved measurements, since the frequency bandwidth of the excitation pulse is almost Fourier transform limited (fwhm $\approx$ 10 cm^{-1}) and too narrow to cover all of the satellites apparently interacting with the S_1 origin level. It is thereby expected that the probed ISC dynamics at the S_1 origin is conduced via the direct SOC with high-v levels in the $T_2(n,\pi^*)$ manifold, of which DOS is sufficiently large even at the moderate excitation energy, e.g., 1000−2000 cm^{-1}.

4.3. Changes in $S_1(\pi,\pi^*)-T_2(n,\pi^*)$ Separation Induced by Microscopic Hydration. The arguments presented in the above section have deduced that the ISC in the AD molecule is dominated by the $S_1(\pi,\pi^*)-T_2(n,\pi^*)$ coupling under jet-cooled conditions, as in the condensed phase.[1−4] Both the $S_1(\pi,\pi^*)$ and $T_2(n,\pi^*)$ states in the AD chromophore will be affected largely by water solvation, and their spectral shifts profoundly correlate to acridone−water(s) geometries (e.g., H bonding sites) in the clusters. Therefore, information on microscopic solvatochromism of $S_1(\pi,\pi^*)$ and $T_2(n,\pi^*)$ is indispensable to elucidate the molecular-scale solvation effects on the nonradiative dynamics of AD. In the preceding paper I, we have already confirmed that the experimental spectral shifts in the $S_1(\pi,\pi^*)$ transition of the hydrated AD clusters are well reproduced via the HOMO−LUMO energetics evaluated by the DFT calculations. We thereby adopt such a naive approach once again in order to estimate how the $T_2(n,\pi^*)$ state in AD is energetically stabilized or destabilized with water association steps and, in particular, in terms of solvation geometry.

According to the MO analysis via the DFT calculation at the B3LYP/6-31G(d,p) level, the next highest occupied molecular orbital (NHOMO) corresponds to the nonbonding orbital (n-orbital) in AD. Thus, we can estimate the spectral shift in the $T_2(n,\pi^*) \leftarrow S_0$ transition from the NHOMO−LUMO energy difference by comparing that calculated for bare AD. Here the solvation shifts are assumed to be exactly equal in the $^1(n,\pi^*)$ and $^3(n,\pi^*)$ states. The spectral shifts in $T_2(n,\pi^*)$ thus calculated for the observed fluorescent AD−$(H_2O)_{1-5}$ **I** clusters (C═O bonded types for $n = 1$ and 2, bridged-types for $n = 3-5$) are plotted against the number of solvents in Figure 10, together with the observed and calculated spectral shifts for the $S_1(\pi,\pi^*)$ transition. At the present stage, the location of the $T_2(n,\pi^*)$ state in bare AD is not known exactly but estimated to be 1000−2000 cm^{-1} below the $S_1(\pi,\pi^*)$ state, so we tentatively set the $S_1(\pi,\pi^*)-T_2(n,\pi^*)$ separation of bare AD to 1000 cm^{-1} in this figure. The calculated spectral shifts in the lowest (π,π^*) and (n,π^*) transitions, and the change in energy difference between the $S_1(\pi,\pi^*)$ and $T_2(n,\pi^*)$ states, i.e., $\delta\Delta E(n,\pi^* - \pi,\pi^*) = \Delta\nu(n,\pi^*) - \Delta\nu(\pi,\pi^*)$, are summarized in Table 3. Despite the oversimplified theoretical approach adopted here, the $T_2(n,\pi^*)$ spectral shifts calculated for the observed hydrated AD conformers with $n = 1-5$ (species B−F) have pointed out an important trend: the H-bonding effects on the $T_2(n,\pi^*)$ state can be classified into two groups on the basis of the water-solvation structures, i.e., C═O bonded types for $n = 1$ and 2, and bridged types for $n = 3-5$.

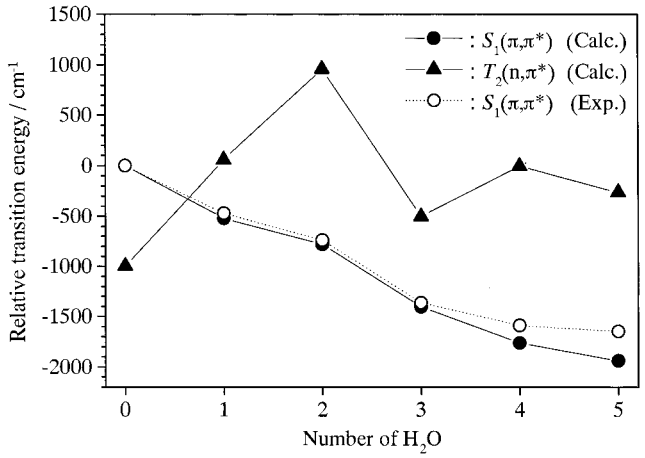

Figure 10. $S_1(\pi,\pi^*)$ and $T_2(n,\pi^*)$ spectral shifts for the observed fluorescent AD−$(H_2O)_{1-5}$ **I** clusters (C═O bonded types for $n = 1$ and 2, bridged-types for $n = 3-5$) plotted against the number of solvents. The observed values for $S_1(\pi,\pi^*)$ are taken from paper I. The calculated $S_1(\pi,\pi^*)$ and $T_2(n,\pi^*)$ shifts are estimated as the HOMO− and NHOMO−LUMO orbital energy differences at the DFT/B3LYP/6-31G(d,p) level, respectively. The difference for the two states in bare AD is arbitrarily set to 1000 cm^{-1}.

(1) n = 1 and 2. In the 1:1 and 1:2 hydrated clusters, where water(s) is σ-type H-bonded to the lone-pair electrons of the carbonyl oxygen (henceforth denoted as "σ-type H-bond conformation"), the estimated blue shifts for $T_2(n,\pi^*)$ are very large (1058 and 1959 cm^{-1}, respectively). This has been well rationalized as the H-bond strength in the excited (n,π^*) state is weakened to much extent in comparison with the ground state, owing to the removal of one of the lone-pair electrons in the excited state. Such an H-bonding interaction has been ascribed to the origin of large blue shifts observed for $\pi^* \leftarrow n$ transitions in solution.[8] On the other hand, the calculated spectral shifts of $S_1(\pi,\pi^*)$ in $n = 1$ and 2 are negative: −520 and −782 cm^{-1}, respectively. Therefore, the changes in the S_1-T_2 separation are quite large in the very beginning of hydration step: $\delta\Delta E(n,\pi^*-\pi,\pi^*) = 1578$ cm^{-1} for a single water association and 2741 cm^{-1} for two waters in the C═O bonded conforma-

TABLE 3: DFT/B3LYP/6-31G(d,p)-Calculated Spectral Shifts in the Lowest (π,π^*) and (n,π^*) Transitions, and Their Differences (cm^{-1}) in Acridone$-(H_2O)_n$ ($n = 1-5$)

species[a]	$\Delta\nu(\pi,\pi^*)$[b]	$\Delta\nu(n,\pi^*)$[b]	$\delta\Delta E(n,\pi^*-\pi,\pi^*)$[c]
AD$-(H_2O)_1$			
I	−520	+1058	+1578
II	−567	−116	+451
AD$-(H_2O)_2$			
I	−782	+1959	+2741
II	−800	−374	+426
AD$-(H_2O)_3$			
I	−1405	+497	+1902
II	−1019	+1994	+3013
III	−843	−336	+507
AD$-(H_2O)_4$			
I	−1764	+995	+2759
II	−969	−264	+705
III	−498	−144	+354
AD$-(H_2O)_5$			
I	−1940	+738	+2678
II	−1864	+934	+2798
III	−608	−351	+257

[a] Species notations are presented in paper I. [b] Relative to the calculated electronic transition energy of bare AD. $\Delta\nu(\pi,\pi^*)$ and $\Delta\nu(n,\pi^*)$ are estimated from the HOMO−LUMO and NHOMO−LUMO enegetics, respectively. [c] $\delta\Delta E(n,\pi^* - \pi,\pi^*) = \Delta\nu(n,\pi^*) - \Delta\nu(\pi,\pi^*)$.

tions. Because the $\Delta E(S_1-T_2)$ value of bare AD has not been determined experimentally (it may be in the range of 1000−2000 cm^{-1}), it is a very delicate problem whether the energy-level inversion between $S_1(\pi,\pi^*)$ and $T_2(n,\pi^*)$ takes place or not in the $n = 1$ cluster (species B). In any case, $|\Delta E(S_1-T_2)|$ is estimated to be smaller than 500 cm^{-1}, yielding to much stronger SOC matrix element between the two states than in bare AD. Therefore, vibronic bands in the T_2 manifold are observable if they are located below the S_1 origin. However, no satellite bands have been observed in vicinity of the S_1 origin by the HB measurement (see Figure 7b), strongly implying that the T_2 origin becomes higher in energy for the $n = 1$ cluster. If this is the case, identification of the triplet bands must be difficult because of the spectral congestion from low-frequency vdW modes, even though they may have detectable intensity. Inversion of the energy ordering between $S_1(\pi,\pi^*)$ and $T_2(n,\pi^*)$ is also consistent with the drastic change in the ISC rate induced by hydration, as mentioned in the next section. On the contrary to $n = 1$, the $\delta\Delta E(n,\pi^* - \pi,\pi^*)$ value for $n = 2$ estimated from the DFT-evaluated (N)HOMO−LUMO energetics is certainly larger than $\Delta E(S_1-T_2)$ of bare AD (<2000 cm^{-1}), and there is little doubt about the energy-level inversion between $S_1(\pi,\pi^*)$ and $T_2(n,\pi^*)$ in the cluster.

(2) $n = 3-5$. As listed in Table 3, all of the calculated values of $\delta\Delta E(n,\pi^* - \pi,\pi^*)$ at these aggregation levels are larger than that in the $n = 1$ cluster, hence $T_2(n,\pi^*)$ must be located above $S_1(\pi,\pi^*)$ in the bridged-type $n = 3-5$ clusters. This estimation is consistent with the HB measurements on the clusters, which ruled out the existence of satellite peaks due to the S_1-T_2 SOC. However, individual spectral shifts for the $S_1(\pi,\pi^*)$ and $T_2(n,\pi^*)$ excitations are definitively altered from those in the 1:1 and 1:2 clusters, as seen in Table 3. The (n,π^*) transition in the $n = 3$, 4, and 5 clusters also shows a blue shift, but the values (497, 995, and 738 cm^{-1}, respectively) are much smaller than that in the C═O bonded $n = 2$ cluster. On the other hand, the red shift in the (π,π^*) transition is much larger in the bridged-type isomers than the lower-size clusters, as has already been addressed in paper I. Consequently, the large positive values in $\delta\Delta E(n,\pi^* - \pi,\pi^*)$ are mostly contributed by the stabilization in $S_1(\pi,\pi^*)$, not by the destabilization in $T_2(n,\pi^*)$.

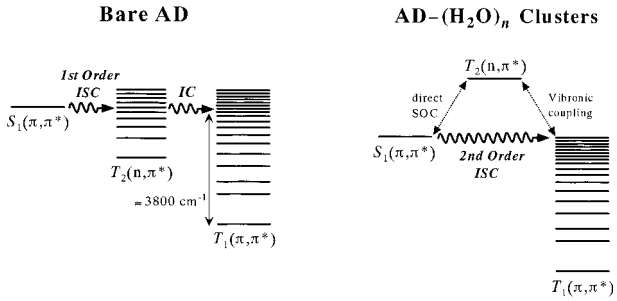

Figure 11. Schematic representation for switching of the ISC mechanism in the AD chromophore by water solvation. In bare AD (left), ISC is proceeded via first-order spin−orbit coupling between the $S_1(\pi,\pi^*)$ and $T_2(n,\pi^*)$ states, while the destabilization of $T_2(n,\pi^*)$ in the hydrated clusters prohibits the direct coupling and the dominant nonradiative pathway is the second-order ISC to the $T_1(\pi,\pi^*)$ manifold, which is mediated by the T_2-T_1 vibronic coupling.

Such a large difference in $S_1(\pi,\pi^*)-T_2(n,\pi^*)$ energetics is definitely correlated to the change of cluster geometry and H-bonding nature. In contrast to the σ-type H-bond conformation in $n = 1$ and 2, a conformation of water molecules forms a kind of π-type H-bond to the carbonyl oxygen in the bridged-type structures, referred to as the "π-type H-bond conformation" [see AD$-(H_2O)_{3-5}$ **I** in Figures 5−7 of paper I]. As the water does not contact directly with the carbonyl lone pair electrons, it is natural that H-bonding effects on the n-orbital are much smaller in the π-type conformation, but destabilization by this type of H-bonding requires more involved explanation. Similar theoretical results have been reported for the H-bonding effects on the (n,π^*) transition in the formaldehyde−water complex, which has been repeatedly chosen as a theoretical model system because of its simplicity.[32−39] By employing the electron−hole potential method,[32,33] Iwata and Morokuma have shown that the $^3(n,\pi^*)$ excitation energy in H_2CO-H_2O is increased by 1420 cm^{-1} where H_2O lies in the H_2CO molecular plane and forms a σ-type H bond to the carbonyl oxygen. On the other hand, in the π-type H bond conformation, the $^3(n,\pi^*)$ excitation also shows a blue shift but its magnitude ($\approx$560 cm^{-1}) is much smaller than that of the σ-type H bond conformation.

The abrupt reduction in the $T_2(n,\pi^*)$ destabilization from $n = 2$ to 3 caused by the crossover in water−solvation structure (C═O bonded chain-type → bridged-type) is clearly reflected in the nonradiative dynamics of the AD chromophore in the hydrated clusters as mentioned below. It is noted that the calculated $\delta\Delta E(n,\pi^* - \pi,\pi^*)$ becomes slightly decreased from $n = 4$ to 5, but this change must be spuriously caused by inaccuracy in calculation, as suggested by the larger discrepancies between the observed and calculated $\Delta\nu(S_1)$ for the larger-size clusters, especially $n = 5$. Also, we have to say that the present estimation of the $\delta\Delta E(n,\pi^* - \pi,\pi^*)$ values seems to be too crude for a detailed comparison between the different types of conformation, as evidenced in the following section.

4.4. Influence of Microscopic Hydration on ISC Dynamics of AD. The results of the fluorescence-lifetime measurements of bare AD and its hydrated clusters indicate that the fluorescence lifetimes (τ_f) of the AD chromophore are sensitively affected by microscopic water solvation. The most drastic change appears at the first association step: τ_f shows an increase more than 2 orders of magnitude from bare AD to the $n = 1$ cluster, while the differences in τ_f among the clusters are less than a factor of 10. Definitely, these pronounced solvation effects on the ISC process are related to the S_1-T_2 energetics in the hydrated clusters as discussed in section 4.3. When the T_2 state is located above the S_1 state, the direct ISC via the

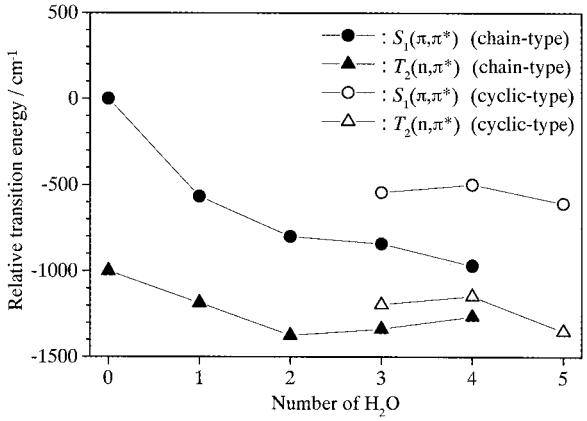

Figure 12. Estimated $S_1(\pi,\pi^*)$ and $T_2(n,\pi^*)$ spectral shifts for the N−H bonded conformers with the chain- ($n = 1-4$) and cyclic-type ($n = 3-5$) water units plotted against the number of solvents. Other details are the same as in Figure 10.

first-order SOC between $^1(\pi,\pi^*)$ and $^3(n,\pi^*)$ is prohibited and the isoenergetic relaxation is contributed predominantly by the indirect ISC between the $S_1(\pi,\pi^*)$ and $T_1(\pi,\pi^*)$ state. As the first-order terms are vanishing for the $^1(\pi,\pi^*)-^3(\pi,\pi^*)$ coupling, the SOC matrix elements for the S_1-T_1 ISC are in the second-order mediated by the vibronic coupling between $T_2(n,\pi^*)$ and $T_1(\pi,\pi^*)$,[7] which should be much smaller than those for $S_1(\pi,\pi^*)-T_2(n,\pi^*)$. The >100-fold reduction in the ISC rates is thus ascribed to the "ISC mechanism switching" in the relaxation pathway, as schematically illustrated in Figure 11.

The variation in τ_f for the hydrated clusters is also well explained in terms of the S_1-T_2 energetics estimated in the previous section. As the $\Delta E(T_2-T_1)$ interval increases, the second-order SOC matrix elements become smaller due to the reduced vibronic mixing between the T_2 and T_1 states. This results in further increase of τ_f, as has been evidenced in the change from $n = 1$ to 2. Roughly speaking, the matrix element for the second-order SOC is inversely proportional to the energy interval,[7,8] thus the change in τ_f is no more drastic as that for the first hydration step. The most notable is the observed small falloff in τ_f from $n = 2$ to 3 (10.9 ns → 7.7 ns). This is *not* an accidental result. The energy shifts in $S_1(\pi,\pi^*)$ and $T_2(n,\pi^*)$ by microscopic hydration are consistent with such fluorescence lifetime behavior: the calculated $\delta\Delta E(n,\pi^* - \pi,\pi^*)$ of $n = 3$ (1902 cm^{-1}) is smaller than that for $n = 2$ (2741 cm^{-1}). This observation clearly indicates a strong correlation between the ISC dynamics in the hydrated AD clusters and the crossover in the structural motifs from the C═O bonded to the bridged forms. For higher aggregation levels (i.e., $n \geq 3$), the ISC rates gradually decrease with increasing degrees of hydration and their changes in each association step become smaller, implying that the variation in $\Delta E(S_1-T_2)$ is going to cease as the cluster sizes become larger. This is consistent with the similarity in the cluster geometry for all the higher sizes, where the water bridge on the AD aromatic rings is connecting between the N−H and C═O sites. As was briefly mentioned in section 4.3, the present approach based on the (N)HOMO−LUMO energetics is too simple for quantitative discussion on the (π,π^*) and (n,π^*) shifts. For example, the estimated $\delta\Delta E(n,\pi^* - \pi,\pi^*)$ for the bridged $n = 5$ conformer is smaller than that for the C═O bonded $n = 2$, contradicting the experimental observation of the longer τ_f for the former. The present calculated results seem to underestimate the $\delta\Delta E(n,\pi^* - \pi,\pi^*)$ in the bridged forms, especially for the higher clusters. Evidently, more accurate calculations on the excited states are needed for definite discussion.

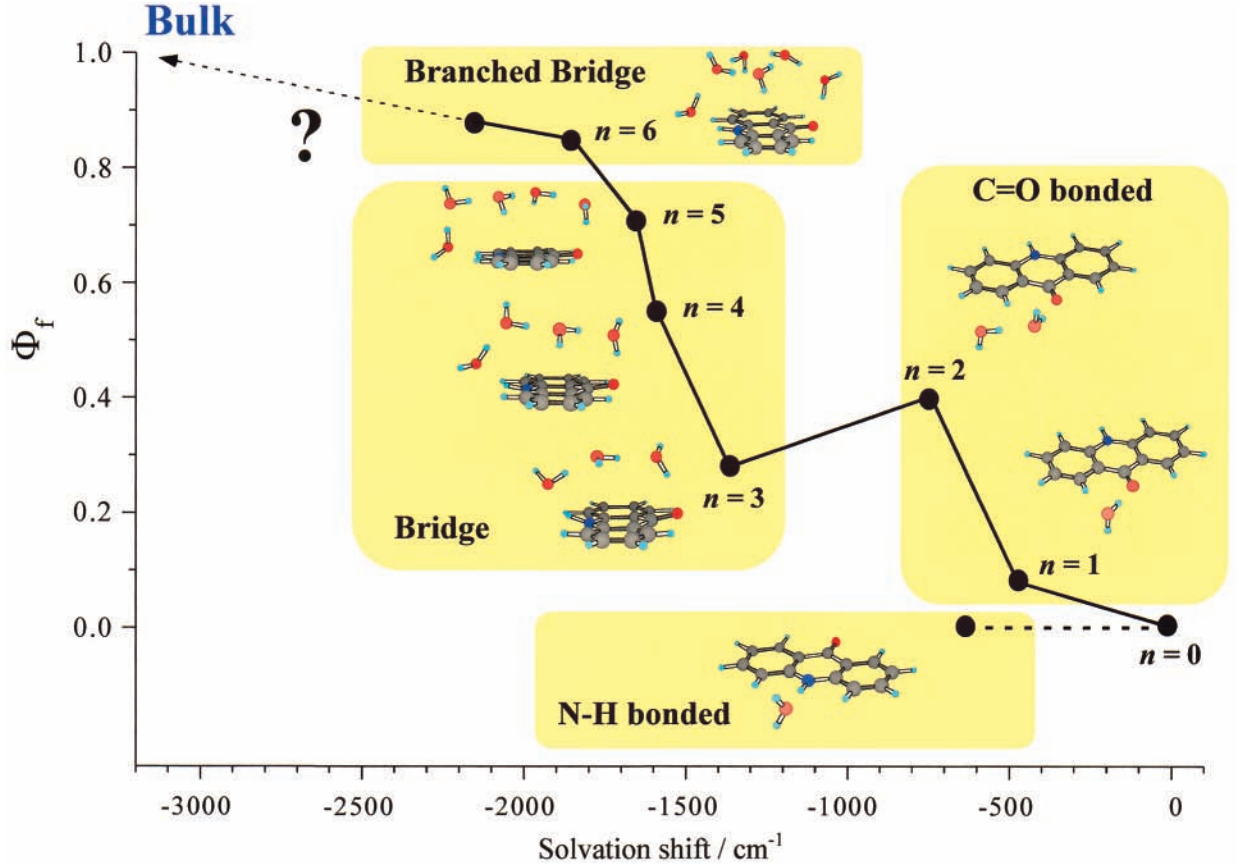

Figure 13. Plots of the estimated fluorescence quantum yields of bare AD and its hydrated clusters as a function of their solvation shifts relative to the origin of bare AD (27265 cm^{-1}), together with pictorial evolution of the water solvation structures in the clusters.

4.5. Influence of Microscopic Hydration in the Other Hydrated AD Conformers. In section 3.4, we presented the observation of the nonfluorescent hydrated AD cluster(s) in the AD−$(H_2O)_1$ mass via the delayed ionization method. The ISC in these cluster(s) should be extremely fast as bare AD, and this implies that water molecule(s) should be bound to H-bonding site(s) of AD whose water solvation has *no* effect on the ISC dynamics in the solute. Apparently, the N−H group is of this type. In Figure 12, the $S_1(\pi,\pi^*)$ and $T_2(n,\pi^*)$ spectral shifts estimated for the N−H bonded chain-type conformers ($n = 1-4$) and the N−H bonded cyclic-type conformers ($n = 3-5$) are plotted against the number of waters. These spectral shifts have also been calculated via HOMO- and NHOMO−LUMO energetics, as explained in section 4.3. In contrast to the C═O bonded- and bridged-type isomers (see Figure 10), when water molecules are exclusively bound to the N−H site, the $S_1(\pi,\pi^*)-T_2(n,\pi^*)$ energy separation shows small change from that of bare AD, irrespective of cluster size and structure of water moiety. This fact strongly suggests that the ISC process of AD is not suppressed in the N−H bonded conformers, and we can conclude that the observed nonfluorescent cluster(s) are some N−H bonded hydrate(s), probably AD−$(H_2O)_1$ **II**, AD−$(H_2O)_2$ **II**, and/or AD−$(H_2O)_3$ **III**, as they should be the most or the second most stable among the conformers with the same sizes. At the present stage, we cannot determine the cluster size of the N−H bonded hydrate(s), because fragmentation of water molecule(s) may take place after the ISC. Further experimentation is needed to discuss the conformer(s) in more detail, and ion-detected infrared spectroscopy implemented with the delayed ionization seems to be the best methody by which to determine both the cluster structure and size at a time, as for the case of the indole−$(H_2O)_2$ cluster.[40] Predissociation dynamics after the fast ISC is also an interesting subject to be studied.

5. Conclusion

Perspective of Microscopic Solvation Effects on Nonradiative Dynamics of Acridone. In Figure 13, we summarize schematically the stepwise evolution in correlation between H-bonding nature and fluorescence property with increasing degrees of solvation, which have been elucidated for acridone and its hydrated clusters in this series of papers I−III. Several important aspects of site-specific intermolecular (H-bonding) interactions, which will also play an important role in bulk water, can be seen in Figure 13. First, the local solute−solvent interaction, which brings the most drastic change to the ISC dynamics, is the σ-type C═O···H−O H-bonding identified in the 1:1 and 1:2 hydrates (species B and C). Despite that only one or two water molecules are involved in solvation, the fluorescence quantum yields in the σ-type H-bonded conformations (0.08 and 0.40 for $n = 1$ and 2, respectively) are almost in the same order with that of AD in bulk water (where $\Phi_f \approx 1.0$). Therefore, the dominant part in the ISC process of AD seems to be governed by the σ-type C═O···H−O H-bonding interaction, which causes the extremely large blue shift in the $T_2(n,\pi^*)$ state as mentioned in section 4.3.

The fluorescence quantum yields of the 1:1 and 1:2 hydrates do not still reach that of AD in water, while the bridge-type conformers show further increasing Φ_f with progressing hydration (0.28, 0.55, and 0.71 for $n = 3$, 4, and 5, respectively). Though T_2 destabilization is not so efficient because of the weak π-type H bond to the carbonyl group, the H-bonding interaction involving π-electron clouds provides an extremely large stabilization to the $S_1(\pi,\pi^*)$ state in the conformations. These facts suggest that the π-H bond interactions also make an essential contribution to achieve the complete suppression of the ISC in AD, which is realized in polar solvents such as water. The fluorescence yield of the most red shifted cluster (species N), whose water solvation number must be ca. 10, already approaches 0.88. This observation reveals that solvation effects on the ISC dynamics of AD are almost completed for relatively small hydration numbers and also implies that closure of the solvent shell around the AD molecule may not be necessary for the unity Φ_f value to be reached.

At low aggregation levels, i.e., $n \leq 3$, H-bonding exclusively associated to the N−H group has also been identified. Actually, relative stability for these isomers is estimated to be at least the same as that for the C═O bonded counterparts. The N−H bonded forms exhibit virtually no microscopic hydration effects on the ISC: their Φ_f must almost vanish as for bare AD. This fact is naturally rationalized as little perturbation on the nonbonding electrons mostly localized at the carbonyl site. The contrasting fluorescence behavior of the C═O and N−H bonded conformers demonstrates the site-specific modification of molecular electronic wave functions. H-bonding networks with a large preference of one site against another with almost the same binding energy cannot be achieved in bulk phases, but such selective H-bonding may have some importance in inhomogeneous environments that possess organized microscopic structures.

Acknowledgment. The present work has been supported by Grants-in-Aid (Nos. 08454177 and 10440172) from the Ministry of Education, Science, Culture, and Sports of Japan. Additional support has been provided from Japan Science and Technology Corporation (JST). Y.O. thanks the Mitsubishi Chemical Foundation and the Japan Securities Scholarship Foundation for financial support.

References and Notes

(1) Siegmund, M.; Bendig, J. *Ber. Bunsen-Ges. Phys. Chem.* **1978**, *82*, 1061.
(2) Kokubun, H.; Kobayashi, M. *Z. Phys. Chem. Neue Folge.* **1964**, *41*, 245.
(3) Fushimi, K.; Kikuchi, K.; Kokubun, H. *J. Photochem.* **1976**, *5*, 457.
(4) Kokubun, H. *Z. Phys. Chem. Neue Folge.* **1976**, *101*, 137.
(5) Val'kova, G. A.; Shcherbo, S. N.; Shigorin, D. N. *Docl. Acad. Nauk USSR* **1978**, *240*, 491.
(6) El-Sayed, M. A.; Kasha, M. *Spectrochim. Acta* **1959**, *15*, 758.
(7) Avouris, P.; Gelbart, W. M.; El-Sayed, M. A. *Chem. Rev.* **1977**, *77*, 793.
(8) Turro, N. *Modern Molecular Photochemistry*; Benjamin-Cummings: Menlo Park, CA, 1978.
(9) Duncan, M. A.; Dietz, T. G.; Liverman, M. G.; Smalley, R. E. *J. Phys. Chem.* **1981**, *85*, 7.
(10) Hiraya, A.; Achiba, Y.; Kimura, K.; Lim, E. C. *J. Chem. Phys.* **1984**, *81*, 3345.
(11) Meijer, G.; Vries, M. S.; Hunziker, H. E.; Wendt, H. R. *J. Phys. Chem.* **1990**, *94*, 4394.
(12) Lipert, R. J.; Colson, S. D. *J. Phys. Chem.* **1990**, *94*, 2358.
(13) Abe, H.; Kamei, S.; Mikami, N.; Ito, M. *Chem. Phys. Lett.* **1984**, *109*, 217.
(14) Ishida, T.; Fujimura, Y.; Fujiwara, T.; Kajimoto, O. *Chem. Phys. Lett.* **1998**, *288*, 433.
(15) Mitsui, M.; Ohshima, Y.; Ishiuchi, S.; Sakai, M.; Fujii, M. *Chem. Phys. Lett.* **2000**, *317*, 211.
(16) Strickler, S.; Berg, R. *J. Chem. Phys.* **1962**, *37*, 814.
(17) Hirayama, S.; Iuchi, Y.; Tanaka, F.; Shobatake, K. *Chem. Phys. Lett.* **1990**, *144*, 401.
(18) Kono, M.; Kubo, Y.; Hirayama, S.; Shobatake, K. *Chem. Phys. Lett.* **1992**, *198*, 214.
(19) Ishijima, S.; Higashi, M.; Yamaguchi, H.; Kubota, M.; Kobayashi, T. *J. Electron. Spectrosc. Relat. Phenom.* **1996**, *82*, 71.
(20) Mitsui, M.; Ohshima, Y.; Ishiuchi, S.; Sakai, M.; Fujii, M., to be published.
(21) Inoue, H.; Hoshi, T.; Yoshino, J. *Bull. Chem. Soc. Jpn.* **1972**, *45*, 2653.
(22) Sneh, O.; Cheshnovsky, O. *J. Phys. Chem.* **1991**, *95*, 7154.

(23) Ottinger, C.; Vilesov, A. F.; Winkler, T. *Chem. Phys. Lett*. **1993**, *208*, 299.
(24) Baba, M.; Kamei, T.; Kiritani, M.; Yamauchi, S.; Hirota, N. *Chem. Phys. Lett*. **1991**, *185*, 354.
(25) Kamei, S.; Sato, T.; Mikami, N.; Ito, M. *J. Phys. Chem*. **1986**, *90*, 5615.
(26) Ohmori, N.; Suzuki, T.; Ito, M. *J. Phys. Chem*. **1988**, *92*, 1086.
(27) Mitsui, M.; Ohshima, Y.; Kajimoto, O., to be published.
(28) Felker, P. M.; Zewail, A. H. *Chem. Phys. Lett*. **1983**, *94*, 448. Felker, P. M.; Zewail, A. H. *Chem. Phys. Lett*. **1983**, *94*, 454.
(29) Wanna, J.; Bernstein, R. *J. Chem. Phys*. **1987**, *86*, 6707.
(30) Nimlos, M. R.; Kelley, D. F.; Bernstein, E. R. *J. Phys. Chem*. **1989**, *93*, 643.
(31) Sidman, J. *J. Chem. Phys*. **1958**, *29*, 644.
(32) Iwata, S.; Morokuma, K. *Chem. Phys. Lett*. **1973**, *19*, 94.
(33) Iwata, S.; Morokuma, K. *J. Am. Chem. Soc*. **1973**, *95*, 7563.
(34) Jeu, W. H. *Chem. Phys. Lett*. **1970**, *7*, 153.
(35) Jeu, W. H. *Mol. Phys*. **1970**, *18*, 31.
(36) Del Bene, J. E. *J. Am. Chem. Soc*. **1973**, *95*, 6517.
(37) Blair, J. T.; Westrook, J. D.; Levy, R. M.; Krogh-Jespersen, K. *Chem. Phys. Lett*. **1989**, *154*, 531.
(38) Ha, T. K.; Makarewicz, J.; Bauder, A. *J. Phys. Chem*. **1993**, *97*, 11415.
(39) Fukunaga, H.; Morokuma, K. *J. Phys. Chem*. **1993**, *97*, 59.
(40) Carney, J. R.; Hagemeister, F. C.; Zwier, T. S. *J. Chem. Phys*. **1998**, *108*, 3379.